ARTICLE OPEN

Check for updates

Grey and white matter microstructure is associated with polygenic risk for schizophrenia

Eva-Maria Stauffer[1✉], Richard A. I. Bethlehem[1,6], Varun Warrier[1,6], Graham K. Murray[1,2,3], Rafael Romero-Garcia[1], Jakob Seidlitz[4,5] and Edward T. Bullmore[1,2]

© The Author(s) 2021

Recent discovery of approximately 270 common genetic variants associated with schizophrenia has enabled polygenic risk scores (PRS) to be measured in the population. We hypothesized that normal variation in PRS would be associated with magnetic resonance imaging (MRI) phenotypes of brain morphometry and tissue composition. We used the largest extant genome-wide association dataset ($N = 69{,}369$ cases and $N = 236{,}642$ healthy controls) to measure PRS for schizophrenia in a large sample of adults from the UK Biobank ($N_{max} = 29{,}878$) who had multiple micro- and macrostructural MRI metrics measured at each of 180 cortical areas, seven subcortical structures, and 15 major white matter tracts. Linear mixed-effect models were used to investigate associations between PRS and brain structure at global and regional scales, controlled for multiple comparisons. Polygenic risk was significantly associated with reduced neurite density index (NDI) at global brain scale, at 149 cortical regions, five subcortical structures, and 14 white matter tracts. Other microstructural parameters, e.g., fractional anisotropy, that were correlated with NDI were also significantly associated with PRS. Genetic effects on multiple MRI phenotypes were co-located in temporal, cingulate, and prefrontal cortical areas, insula, and hippocampus. Post-hoc bidirectional Mendelian randomization analyses provided preliminary evidence in support of a causal relationship between (reduced) thalamic NDI and (increased) risk of schizophrenia. Risk-related reduction in NDI is plausibly indicative of reduced density of myelinated axons and dendritic arborization in large-scale cortico-subcortical networks. Cortical, subcortical, and white matter microstructure may be linked to the genetic mechanisms of schizophrenia.

Molecular Psychiatry; https://doi.org/10.1038/s41380-021-01260-5

INTRODUCTION

A substantial genetic contribution to the pathogenesis of schizophrenia is indicated by twin and familial heritability estimates of ~80% [1–3], and single nucleotide polymorphism (SNP) heritability of ~24% [4]. The most recent genome-wide association study (GWAS) identified 270 risk-associated loci, allowing the construction of polygenic risk scores (PRS) that explain up to 7.7% of the variance in schizophrenia [4]. PRS are normally distributed in the general population and have been used to investigate the shared genetics between schizophrenia, neurodevelopmental trajectories, and brain morphology [5].

The genetic liability for schizophrenia is thought to cause proximal changes in brain structure and function [6], which then result in distal changes in psychological function and clinical symptoms characteristic of schizophrenia [7–10]. Although brain structural abnormalities have been consistently reported in schizophrenia case-control studies [11–13], and are substantially heritable [14–16], the current evidence linking magnetic resonance imaging (MRI) markers of brain structure to polygenic risk for schizophrenia is inconsistent [17]. Recent studies reported no significant associations between PRS and volume of subcortical nuclei [18–20], or between PRS and white matter structure [18]. Some studies have reported significant negative associations between PRS and global brain measures, such as total white matter volume [21] or mean cortical thickness (CT) [22]; but effect sizes have been small ($R^2 = 0.2\%$) and not consistently significant between studies [17, 18]. Thickness of insular cortex was specifically associated with polygenic risk for schizophrenia ($R^2 = 0.2\%$) [22] but most prior studies have not found significant associations between PRS and regional brain anatomy [17].

The current lack of clear evidence for an association between genetic risk for schizophrenia and brain structure could be attributable to the relatively small sample sizes of prior genetic neuroimaging studies ($100 < N < 15{,}000$), which were likely underpowered to detect small polygenic effects [17, 18, 20, 22]. Inherently low power is necessarily exacerbated when type 1 error is appropriately adjusted to control for multiple testing of regional phenotypes [22]. It is also notable that cortical and subcortical MRI phenotypes so far investigated have mostly been macrostructural metrics, e.g., CT, which are coarse-grained compared to the predicted effects of risk genes on tissue composition and cellular organization.

[1]Department of Psychiatry, Cambridge Biomedical Campus, University of Cambridge, Cambridge, UK. [2]Cambridgeshire and Peterborough NHS Trust, Elizabeth House, Fulbourn Hospital, Cambridge, UK. [3]Institute for Molecular Bioscience, University of Queensland, St Lucia, QLD, Australia. [4]Department of Child and Adolescent Psychiatry and Behavioral Science, Children's Hospital of Philadelphia, Philadelphia, PA, USA. [5]Department of Psychiatry, University of Pennsylvania, Philadelphia, PA, USA. [6]These authors contributed equally: Richard A.I. Bethlehem, Varun Warrier. ✉email: ems206@cam.ac.uk

Received: 8 March 2021 Revised: 26 July 2021 Accepted: 30 July 2021
Published online: 30 August 2021

Case-control studies of schizophrenia have consistently reported significant reductions in regional CT, surface area (SA) [12], grey matter volume (Vol) [23], intrinsic curvature (IC, a metric of local connectivity of cortex) [24], and local gyrification index (LGI, a metric of cortical folding) [25]. These are all macrostructural markers of brain morphology that are derived from T1-weighted MRI data and estimated at each cortical or subcortical region. In contrast, microstructural MRI phenotypes are derived from diffusion-weighted imaging (DWI) data, providing finer-grained information about the cellular composition of brain tissue [26–28]. Case-control studies of schizophrenia have increasingly reported significant differences in grey matter microstructure [26], such as increased mean diffusivity (MD) [28–30], decreased fractional anisotropy (FA) [31], decreased neurite density index (NDI) [26] and orientation dispersion index (ODI) [32]. Significant microstructural abnormalities of white matter tracts have also been reported, including decreased FA [13, 33] and NDI [34, 35], and increased MD [13], in schizophrenia case-control studies.

We therefore hypothesized that macro- and microstructural MRI markers of grey and white matter would be associated with polygenic risk for schizophrenia. We analyzed multimodal MRI and genotype data from $N \sim 30{,}000$ participants in the UK Biobank (UKB) to conduct a comprehensive study of PRS association with nine brain MRI phenotypes (Fig. 1). In grey matter, we measured five macrostructural (CT, SA, Vol, LGI, and IC) and four microstructural (FA, MD, NDI, and ODI) MRI metrics in 180 bilateral cortical areas; and a subset of these metrics (Vol, FA, MD, NDI, and ODI) in seven subcortical regions. In white matter, we measured FA, MD, NDI, and ODI in 15 major axonal tracts. We used the largest available GWAS dataset for schizophrenia ($N = 69{,}369$ cases and $N = 236{,}642$ controls) to construct schizophrenia PRS for each subject [4]. We expected that this combination of increased GWAS sample size for PRS estimation, and access to the large UKB sample of MRI measurements of both macro- and microstructural metrics, would enhance statistical power to test the hypothesis that MRI phenotypes are associated with schizophrenia PRS in the population. In light of the significant associations we discovered by these analyses, we were stimulated to conduct post-hoc analyses of the causal relationships between a subset of NDI metrics and schizophrenia, using Mendelian randomization (MR) and genetic correlations.

METHODS AND MATERIALS

Participants

Data were provided by the UK Biobank, a population-based cohort of >500,000 subjects aged between 39 and 73 years [36]. We focused on a subset of $N = 40{,}680$ participants for each of whom complete genotype and multimodal MRI data were available for download (February 2020); Fig. S2. We excluded participants with incomplete MRI data, or with a diagnosis of schizophrenia (self-reported or by ICD-10 criteria). Prior to analysis of each MRI phenotype, we additionally excluded participants who were robustly defined as outliers by global or regional metrics more than five times the median absolute deviation from the sample median (±5 MAD), see SI Methods Sample Selection. Ethical approval was obtained from the Human Biology Research Ethics Committee, University of Cambridge (Cambridge, UK). Informed consent was provided by all participants (https://biobank.ctsu.ox.ac.uk/crystal/field.cgi?id=200).

Imaging acquisition and preprocessing

MRI data acquisition has been described in detail elsewhere [37]. Minimally processed T1- and T2-FLAIR- weighted MRI data (and DWI data) were downloaded from UK Biobank (application 20904) (https://biobank.ctsu.ox.ac.uk/crystal/crystal/docs/brain_mri.pdf) and further processed with Freesurfer (v6.0.1) [38] using the T2-FLAIR weighted images to improve pial surface reconstruction. Pre-processing steps included bias field correction, registration to stereotaxic space, intensity normalization, skull-stripping, and grey/white matter segmentation; Following reconstruction, the Human Connectome Project parcellation [39] was aligned to each individual image and regional metrics were estimated for 180 bilateral cortical areas and seven bilateral subcortical structures. DWI data were co-registered with the T1-aligned parcellation template to estimate FA and MD at each region. Neurite orientation dispersion and density imaging (NODDI) reconstruction was performed using the AMICO pipeline [40]. Probabilistic tractography was used to estimate FA, MD, NDI, and ODI values at each of 15 major white matter tracts defined using AutoPtx [41]. Documentation and code for these processing pipelines is available on Github (https://github.com/ucam-department-of-psychiatry/UKB).

Genotyping and genetic quality control

Genome-wide genotype data were available for $N = 488{,}377$ participants, with DNA acquisition, imputation, and quality control pipelines as described elsewhere [42]. We excluded participants if they were not primarily of white British ancestry based on genetic ethnic grouping and subjects with excessive genetic heterozygosity, genotyping rate ≤95%, mismatch between reported and genetic sex, and genetic relatedness >0.25 between participants [43]. We also excluded SNPs with minor allele frequency ≤0.01, that were not in Hardy–Weinberg equilibrium ($p \le 1 \times 10^{-6}$), variant call rate ≤98%, and an imputation quality score ≤0.4, resulting in 5,366,036 SNPs.

Polygenic risk score

A PRS is calculated by multiplying the number of risk alleles by the effect size of each allele and summing the products over all SNPs for each individual [44]. We used the computationally efficient *P*-value clumping and thresholding method in PRSice 2 [4, 45, 46]. First, SNPs were clumped using the UK Biobank data as a reference panel so that only the most strongly associated SNP in a region was retained ($R^2 = 0.1$, physical distance = 250 kb) [46]. Second, for each participant, we estimated a set of eight PRS with varying SNP-wise probability thresholds for inclusion ($0.0001 < P_{SNP} < 1$) to balance signal to noise ratio [22, 47, 48].

We estimated PRS's for $N = 29{,}879$ participants, using effect sizes for each allele from a trans-ancestry GWAS with $N = 69{,}369$ schizophrenia cases and $N = 236{,}642$ healthy controls, mostly (~80%) of European ancestry [4]. Previous studies that used UK Biobank data to test association of MRI markers with polygenic risk estimated PRS from smaller GWAS datasets of both European and East Asian ancestry [18, 22, 49]. Thus, we estimated eight PRS from the full trans-ancestry GWAS [4] for each participant and found that scores were normally distributed at all P_{SNP} inclusion thresholds (Fig. S3, SI Methods); the number of SNPs included in the PRS calculation at each probability threshold is reported in Table S1.

Statistical analysis of PRS associations with MRI phenotypes

Statistical analyses were conducted in R (version 3.5.2; R Foundation, Vienna, Austria; https://cran.r-project.org/bin/windows/base/old/3.5.2/). We used linear mixed effect (LME, "nlme" package version 3.1-144) models (Equation 1) to estimate the associations between the scaled PRS and each of the scaled MRI phenotypes with covariates including age, age^2, sex, genotype batch, 15 genetic principal components (Data-Field 22006), and *x, y* and *z* coordinates of head position in the scanner to control for static-field heterogeneity (Data-Field 25756-25758) [50]. Hemisphere was fitted as a random effect, resulting in 180 bilateral regions [18, 22, 51], after testing for PRS-by-hemisphere interactions had demonstrated that none were significant at FDR = 5% (Tables S2–S4).

$$\begin{aligned} &MRI\ Phenotype \sim PRS + Age + Age^2 + Batch + \\ &\quad 15\ PCs + x{-}coordinate + y{-}coordinate + \\ &\quad z{-}coordinate, random = \sim 1|Hemisphere \end{aligned} \quad (1)$$

To identify the optimal P_{SNP} thresholds for PRS construction, and to minimize the multiple testing required for comprehensive brain regional mapping of genetic associations, we decided a priori on a two-step analysis for cortical phenotypes. First, we estimated and tested the association of all eight PRS with each MRI metric at a global cortical scale, using the Benjamini–Yekutieli procedure (BY = 5%) to control for multiple tests over all metrics and thresholds. We thus identified the genome-wide probability threshold for PRS inclusion, P_{SNP}-global, that produced the PRS most strongly associated with each global cortical metric. Second, we used the PRS defined by P_{SNP}-global to test for genetic association with the corresponding metric at a regional scale in 180 cortical areas, covarying for total intracranial volume, with the false-discovery rate (FDR) = 5%.

For analysis of the smaller number of subcortical regions (7 regions), and white matter tracts (15 tracts), we tested for association with all eight PRS

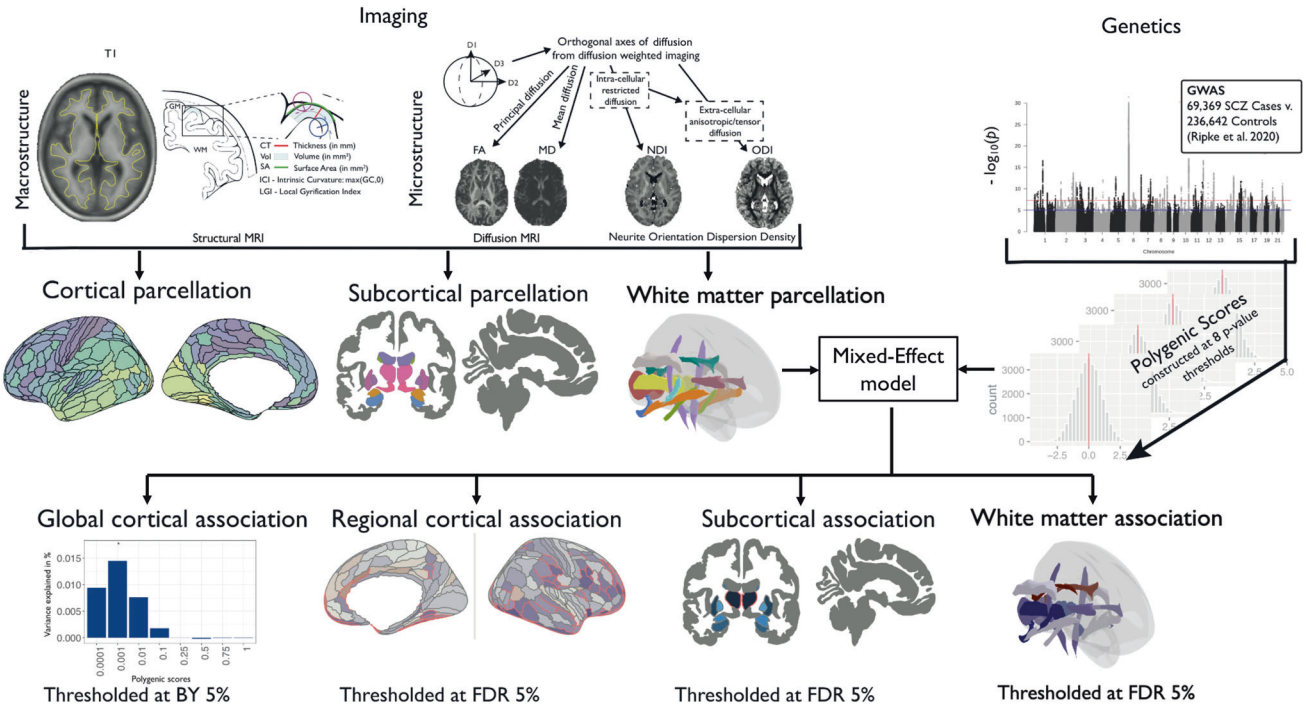

Fig. 1 Schematic summary of the study. We estimated five macrostructural metrics and four microstructural metrics at each of 180 bilateral cortical areas, and on average over all cortical areas, for variable numbers of subjects in the UK Biobank for whom quality-controlled data were available: for cortical thickness (CT), $N = 29{,}778$; surface area (SA), $N = 29{,}777$; grey matter volume (Vol), $N = 29{,}778$; intrinsic curvature (IC), $N = 29{,}676$; local gyrification index (LGI), $N = 27{,}086$; fractional anisotropy (FA), $N = 28{,}232$; mean diffusivity (MD), $N = 28{,}165$; neurite density index (NDI), $N = 27{,}632$; and orientation dispersion index (ODI), $N = 27{,}658$. We also estimated one macrostructural metric and four microstructural metrics at each of seven subcortical regions (amygdala, accumbens, caudate, putamen, pallidum, hippocampus, and thalamus): Vol, $N = 29{,}854$–$29{,}878$; FA, $N = 28{,}192$–$28{,}238$; MD, $N = 27{,}664$–$28{,}154$; NDI, $N = 27{,}590$–$27{,}638$; and ODI, $N = 27{,}600$–$27{,}658$. Additionally, we measured four microstructural metrics at 15 major white matter tracts: FA, $N = 27{,}987$–$28{,}346$; MD, $N = 28{,}327$–$28{,}346$; NDI, $N = 28{,}247$–$28{,}337$; ODI, $N = 28{,}219$–$28{,}346$. Polygenic risk scores for schizophrenia (PRS) were based on GWAS data from 69,396 cases and 236,642 controls and were calculated for each participant at eight P_{SNP}-value thresholds for inclusion of significant variants, using the clumping and thresholding approach [46]. To assess associations between multiple schizophrenia polygenic risk scores and cortical phenotypes, we first used mixed-effect models to identify which P_{SNP}-value threshold(s) produced the PRS most strongly associated with each cortical metric at global scale, controlled for multiple comparisons using the Benjamini–Yekutieli procedure (BY = 5%). We then used mixed-effect models to test the association between the globally most predictive PRS for each metric at each cortical area, controlling for multiple comparisons with the false-discovery rate (FDR) at 5%. For subcortical structures and white matter tracts, we tested for association between each MRI metric and each of eight polygenic risk scores, with FDR = 5%. The Manhattan plot is for illustrative purposes only and based on a previously published schizophrenia GWAS [49], downloaded from https://www.med.unc.edu/pgc/pgc-workgroups/.

at each region, with FDR = 5%, to control for the multiple tests entailed (56 and 120, respectively).

We performed various sensitivity analyses: First, we repeated the regional cortical analysis using the PRS scores at all other P_{SNP} thresholds and showed that significant associations between PRS and regional MRI phenotypes were largely conserved across P_{SNP} thresholds (Figs. S4–S12). Second, we covaried for the corresponding global metric in the LME model of PRS associations with regional metrics, which revealed a highly correlated pattern for regional cortical associations (Fig. S13). Third we repeated cortical analysis using PRS scores from GWAS data in European samples and showed that our findings were not biased by population stratification (SI Methods, Fig. S14-16).

We report the proportion of explained phenotypic variance by the PRS in percentages (R^2) and standardized effect sizes (β) throughout.

Bidirectional Mendelian randomization analyses and genetic correlations

We conducted exploratory bidirectional MR analyses for a subset of imaging phenotypes using the 'twosampleMR' package v0.5.6 in the UK Biobank sample [52]. MR employs genetic instruments to test whether there is a causal effect of the exposure phenotype on the outcome phenotype. We tested two directions of causal relationship: (i) schizophrenia (exposure) causing brain NDI changes (outcome); and (ii) brain NDI changes (exposure) causing schizophrenia (outcome). We restricted MR analysis to a subset of global and regional NDI metrics that were most strongly and robustly associated with schizophrenia PRS and showed ≥ 10 genome-wide significant loci, to ensure reasonable statistical power (Tables S5 and S6).

For MR analysis (i) of the causal effect of schizophrenia on NDI, we used the same GWAS summary statistics as for the PRS analyses [4]. Genetic instruments were chosen at a P threshold of 5×10^{-8} and clumped with a distance of 10,000 kb and LD r^2 of 0.001. These SNPs were then identified within the outcome GWAS and SNP effect of exposure and outcome data were harmonized to match the effect alleles leading to 184 genetic instruments and 41 imaging phenotypes (Table S7).

For MR analysis (ii) of the causal effect of NDI on schizophrenia, we performed GWAS using fastGWA with sample sizes in the range $N =$ 31,722–31,760 for different regional metrics (SI Methods) [53]. Genetic instruments were chosen at two significance thresholds. First, we used a genome-wide significant threshold of $P = 5 \times 10^{-8}$ and clumped with a distance of 10,000 kb and LD r^2 of 0.001. Based on these parameters, 40 NDI phenotypes were included and the number of genome-wide significant loci ranged from three to 29 after harmonizing the data (Table S8). Second, we identified genetic instruments for the same 40 NDI phenotypes with a lower GWAS significance threshold of $P = 5 \times 10^{-6}$, as the smallest number of genetic instruments after data harmonizing was three [47, 54] (Tables S5 and S6). This increased the number of genetic instruments, which ranged from 21 to 71 after data harmonizing (Table S9), which was expected to enhance statistical power for MR analysis at the cost of somewhat less stringent type 1 error control in construction of the instrumental variables.

To fit the models, we used inverse variance-weighted (IVW) MR, which assumes that all SNPs are valid genetic instruments, as the main method to

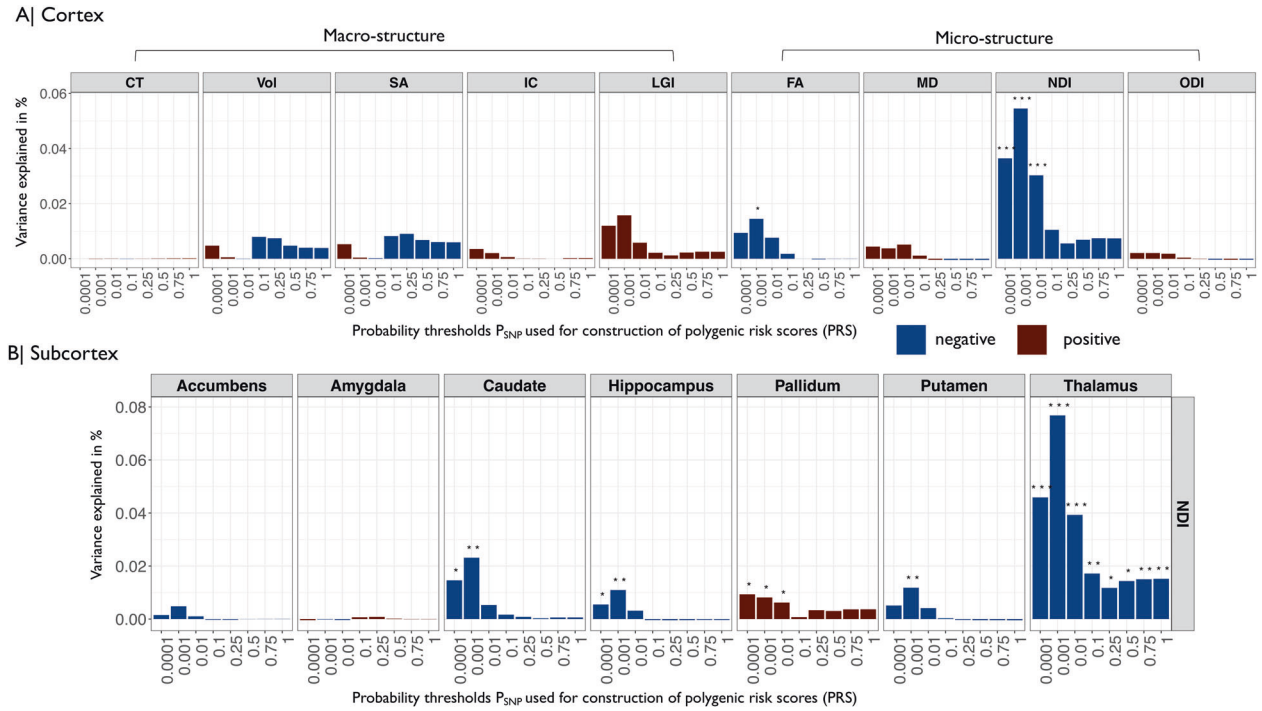

Fig. 2 Associations between polygenic risk scores for schizophrenia and global cortical and regional subcortical metrics of human brain structure. A Barcharts of variance explained by schizophrenia PRS (R^2, *y*-axis) constructed at each of eight probability thresholds ($0.0001 \geq P_{SNP} \leq 1$, *x*-axis) for each of nine global mean cortical metrics: CT cortical thickness, Vol grey matter volume, SA surface area, IC intrinsic curvature, LGI local gyrification index, FA fractional anisotropy, MD mean diffusivity, NDI neurite density index, ODI orientation dispersion index. Blue bars indicate negative associations and red bars positive associations; asterisks indicate *P* values for association after FDR correction: $^*P \leq 0.05$, $^{**}P \leq 0.01$, $^{***}P \leq 0.001$. Polygenic risk scores for schizophrenia were significantly negatively associated with global neurite density index and fractional anisotropy. **B** Barcharts of variance explained by PRS (R^2, *y*-axis) constructed at each of eight probability thresholds ($0.0001 \geq P_{SNP} \leq 1$, *x*-axis) for NDI measured at each of seven subcortical regions (colors and asterisks code sign and significance of association as in **A**). PRS was significantly negatively associated with NDI in thalamus, hippocampus, putamen, and caudate; and significantly positively associated with NDI in pallidum.

estimate causal effects [55]. The robustness of significant findings obtained using IVW was assessed using two additional methods (sensitivity analyses): weighted median (WM) method, which provides consistent results even when 50% of the genetic instruments are invalid; and MR-Egger, which accounts for pleiotropy [55], and we tested for heterogeneity and horizontal pleiotropy.

To evaluate consistency in effect direction, we additionally calculated genetic correlations between schizophrenia and the same 41 imaging phenotypes using Linkage Disequilibrium Score Regression v1.0.1 [56] and corrected for multiple comparison using FDR.

RESULTS

Sample

The sample sizes available after QC for analysis of cortical, subcortical, and white matter structure varied between regions and MRI metrics in the range $N = 27{,}086$–$29{,}878$ (Fig. 1). All samples comprised ~55% female, 45% male participants aged 40–70 years, with mean age ~55 years; see Tables S10–S12 for details.

Global cortical MRI phenotypes

Two global cortical metrics were significantly associated with PRS at one or more P_{SNP}-value thresholds (BY = 5%). Both were microstructural phenotypes derived from DWI or NODDI: FA was significantly negatively associated with the PRS constructed with $P_{SNP} \leq 0.001$; and NDI was significantly negatively associated with PRS constructed at P_{SNP}'s ≤ 0.0001, 0.001, and 0.01 (Fig. 2A and Table S13). These results indicate that participants with increased polygenic risk for schizophrenia have decreased global FA and NDI "on average" over the whole cortex. The association between PRS and NDI was more robust to the choice of probability threshold used to construct the risk score; and PRS accounted for a larger proportion of the variance in NDI (~0.05%), compared to FA (~0.02%) and other metrics.

Regional cortical MRI phenotypes

The macrostructural metrics (CT, SA, Vol) were positively correlated with each other and negatively correlated with LGI. Among the microstructural metrics, NDI and FA were positively correlated; and both were negatively correlated with MD and ODI (Fig. 3A).

There were significant associations between PRS and eight out of nine MRI metrics in at least one cortical area, with the exception being CT (Fig. 3B). The proportion of regional variance explained by PRS varied between metrics in the range $0.002\% \leq R^2 = \leq 0.08\%$ with $-0.03 \leq \beta \leq +0.03$ (Table S14).

Among the microstructural metrics, NDI was significantly associated with PRS in 149 cortical areas (maximum $R^2 = 0.06\%$, $\beta = -0.03$). The top ten areas where NDI was most strongly negatively associated with PRS were located in association auditory cortex, early auditory cortex, ventral visual stream, posterior cingulate cortex, insular and frontal opercular cortex, posterior opercular cortex, inferior parietal cortex, and superior parietal cortex (see Table S15). FA was negatively associated with PRS in 63 regions (maximum $R^2 = 0.01\%$, $\beta = -0.01$); and positively associated with PRS in two regions (maximum $R2 = 0.01\%$, $\beta = 0.01$). The top ten regions where FA was most strongly associated with PRS were all areas of temporal, cingulate, frontal, and insular cortex, where decreased FA was associated with higher risk scores. MD was significantly associated with PRS in 76

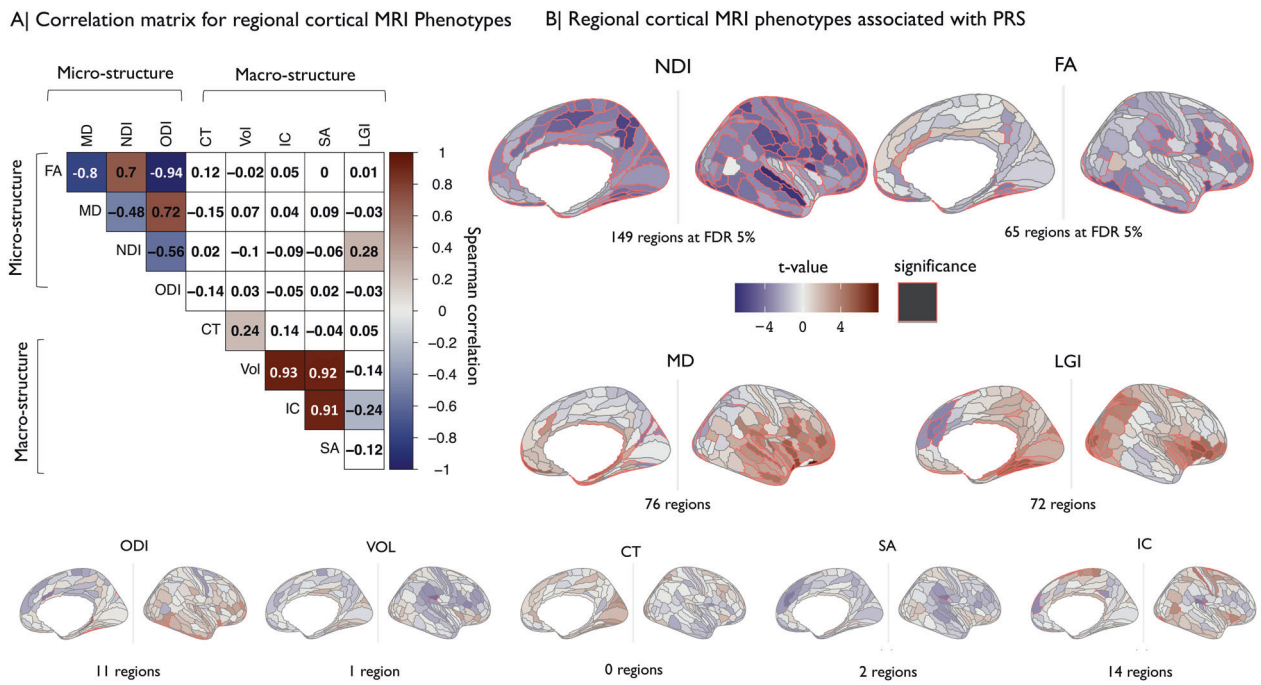

Fig. 3 Regional cortical MRI phenotypes: correlations between metrics and associations of each metric with schizophrenia polygenic risk scores. A Matrix of Spearman's correlation for each pair of nine MRI metrics. Shades of blue indicate significant negative correlations and shades of red indicate significant positive correlations. **B** Cortical *t*-maps representing the strength of association between schizophrenia PRS and regional MRI phenotypes; regions where the effect of PRS is statistically significant at FDR = 5% are outlined in red. NDI and FA metrics, which were globally decreased by genetic risk for schizophrenia (Fig. 2), were significantly regionally decreased in multiple areas. MD and LGI metrics were significantly regionally increased by genetic risk in several areas.

regions (66 positive and 10 negative associations). ODI was the microstructural metric least frequently associated with PRS, at 11 cortical regions.

Of the macrostructural metrics, LGI showed the highest number of significant associations with PRS (72 regions; 67 positive and five negative) compared to Vol, SA, and IC, each of which was significant in less than 15 regions (maximum $R^2 \leq 0.02\%$, maximum $|\beta| \leq 0.01$).

Since the MRI phenotypes were not independent of each other (Fig. 3A), we further explored the spatial co-localization of genetic associations with different cortical metrics. The cortical *t*-maps of PRS association with NDI and FA were significantly positively correlated with each other, and were negatively correlated with the cortical *t*-maps of PRS associations with ODI (both NDI and FA) and MD (FA only) (Fig. 4A). In other words, regions where genetic risk was most strongly associated with decreased FA (FA(t) < 0) tended to be the same regions where PRS was most strongly associated with decreased NDI (NDI(t) < 0) and increased MD (MD(t) > 0; Fig. 4B).

We also simply counted the number of different MRI phenotypes that were significantly associated with PRS at each of 180 cortical areas. There were genetic effects on at least two metrics in 122 regions (Table S16), at least three metrics in 68 regions, and at least four metrics in 21 regions (Fig. 4C). The most frequently co-localized genetic associations were with NDI and MD (63 regions) and NDI and FA (61 regions) (SI Results). Regions that were associated with PRS in terms of multiple MRI phenotypes were located in (inferior) frontal, insular, temporal, auditory, and ventral visual stream areas of cortex (Fig. 4D and Table S16).

Regional subcortical MRI phenotypes

We estimated the association between PRS and one macrostructural (Vol) and four microstructural phenotypes (MD, FA, NDI, ODI) at seven subcortical regions. The single strongest effect was a negative association between PRS and NDI of thalamus ($R^2 = 0.08\%$, $\beta = -0.03$). NDI was also negatively associated with PRS in the caudate, hippocampus, and putamen; and positively associated with PRS in pallidum (Fig. 2B and Table S17). Further significant associations were found between PRS and MD of the amygdala, caudate, hippocampus, pallidum, and putamen; between PRS and Vol of caudate, putamen and hippocampus; between PRS and FA of putamen and thalamus; and between PRS and ODI of pallidum and thalamus (Fig. S17).

Regional white matter phenotypes

We identified a large number of significant associations between PRS and microstructural metrics in 15 white matter tracts: NDI in 14 out of 15 tracts, FA in 12 tracts, MD in 11 tracts, and ODI in 5 tracts (Fig. 5 and Fig. S19). These results indicate that higher genetic risk for schizophrenia is associated with decreased NDI and FA, and increased MD, within callosal fibers, projection fibers, association fibers, limbic system fibers, and brainstem tracts. The highest proportion of phenotypic variance explained by PRS was found for NDI of the forceps minor ($R^2 = 0.12\%$, $\beta = -0.04$) followed by NDI of projection fibers (superior thalamic radiation $R^2 = 0.11\%$, $\beta = -0.03$) and association fibers (inferior fronto-occipital fasciculus $R^2 = 0.10\%$, $\beta = -0.03$). Those associations showed a consistent direction of effect and were significant at all P_{SNP} inclusion thresholds. The strongest negative association between PRS and FA was within the forceps minor ($R^2 = 0.11\%$, $\beta = -0.03$), followed by projection fibers (superior thalamic radiation $R^2 = 0.06\%$, $\beta = -0.02$), and association fibers (anterior thalamic radiation $R^2 = 0.06\%$, $\beta = -0.02$). The strongest positive associations between PRS and MD were located in association fibers (uncinate fasciculus $R^2 = 0.07\%$, $\beta = 0.03$) followed by limbic system fibers (cingulate gyrus part of cingulum $R^2 = 0.04\%$, $\beta = 0.02$) and the forceps minor ($R^2 = 0.03\%$, $\beta = 0.02$) (Table S18).

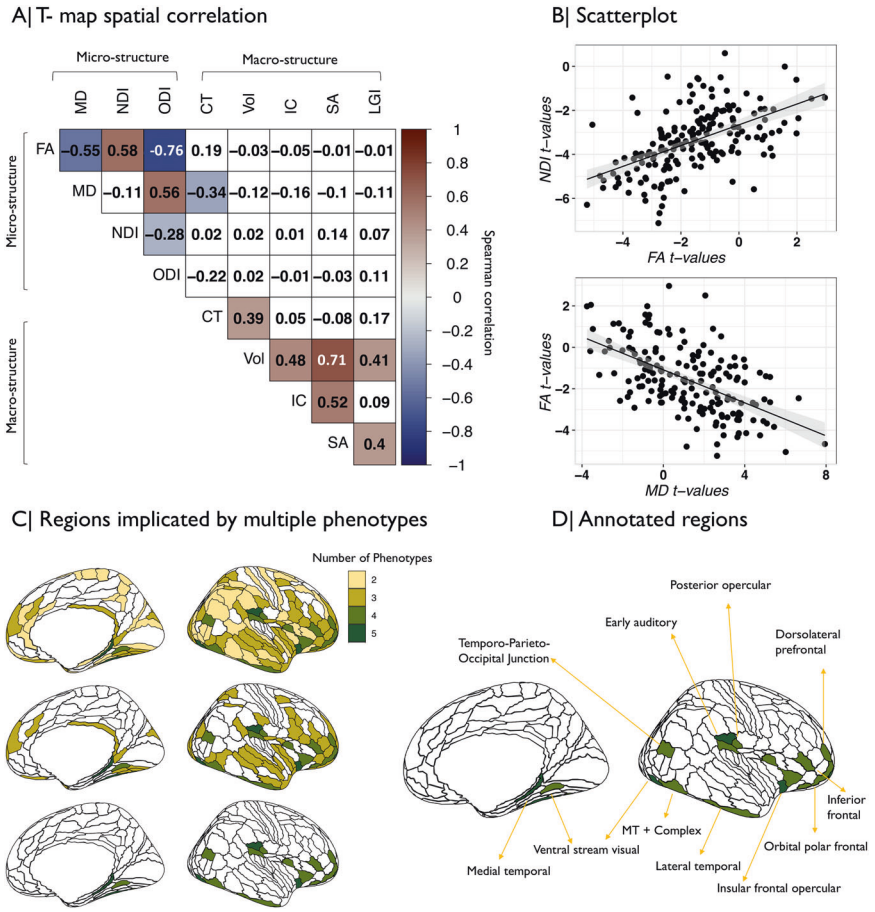

Fig. 4 Anatomical co-localization of polygenic risk effects for schizophrenia on multiple MRI phenotypes. A Matrix of spatial correlations between cortical *t*-maps of association between schizophrenia PRS and nine MRI metrics. **B** Scatterplot showing the relationships between (top) cortical *t*-maps of FA and NDI and (bottom) cortical *t*-maps of FA and MD; each point represents a cortical area. **C** Cortical map color coded to indicate the number of MRI phenotypes that were significantly associated with schizophrenia PRS at each region. Colored regions had at least two (top), three (middle), or four (bottom), MRI phenotypes significantly associated with genetic risk of schizophrenia. **D** The brain regions where schizophrenia PRS was significantly associated with four MRI phenotypes were anatomically located in medial and lateral temporal cortex, ventral visual stream, insular and frontal cortex.

Bidirectional Mendelian randomization on schizophrenia and NDI metrics

For these post-hoc analyses of causality, we focused on 41 NDI phenotypes (global NDI and regional NDI metrics in 21 cortical areas, 5 subcortical nuclei, and 14 white matter tracts). After correction for multiple comparisons, there was no significant evidence for a causal effect of schizophrenia on NDI metrics (MR (i)), and there was no significant evidence for a causal effect of NDI metrics on schizophrenia (MR (ii)) using genetic instruments identified by genome-wide association significance threshold of $P = 5 \times 10^{-8}$ (Tables S7 and S8). However, for MR (ii), when we relaxed the inclusion threshold for genetic instruments to $P = 5 \times 10^{-6}$, we found that lower genetically predicted NDI in the thalamus was associated with increased genetically predicted risk for schizophrenia (IVW method $\beta = -0.16$, $P_{FDR} = 0.02$), suggesting that reduced thalamic NDI may cause increased risk of schizophrenia. Sensitivity analyses using the WM method were also significant ($\beta = -0.14$, $P = 0.002$). NDI of thalamus showed significant heterogeneity between individual genetic variants (P for Q-test < 0.0001) but the Egger intercept was not significant, suggesting no evidence for substantial pleiotropic effects ($P = 0.42$) (Table S9). In addition, leave-one-out analysis did not indicate that the result was driven by any one genetic variant (Fig. S20).

Genetic correlations were modest and did not survive multiple testing correction. However, 80% of the correlations were in the negative direction predicted by significant negative associations between NDI and PRS scores (Table S19).

DISCUSSION

We estimated the strength of association between PRS for schizophrenia and nine MRI phenotypes measured at 180 cortical areas, seven subcortical structures, and 15 white matter tracts. In strong support of our motivating hypothesis, we found that PRS was significantly associated with microstructural metrics of brain tissue composition at global and regional scales of cortex; in the thalamus, basal ganglia, and hippocampus; and extensively in white matter tracts. First, we interpret and integrate these signals of significant association between genetic risk for schizophrenia and brain MRI metrics, especially NDI; then we discuss post-hoc analyses of causality stimulated by these results.

Neurite density index—a plausible brain MRI marker for schizophrenia risk?

Of all nine MRI metrics considered, NDI was the most robustly associated with PRS. NDI is derived from NODDI, an MRI sequence that was developed to estimate the microstructural complexity of dendrites and axons— collectively referred to as neurites—in grey and white matter of the living brain. NODDI compartmentalizes tissue into three microstructural environments—intra-cellular,

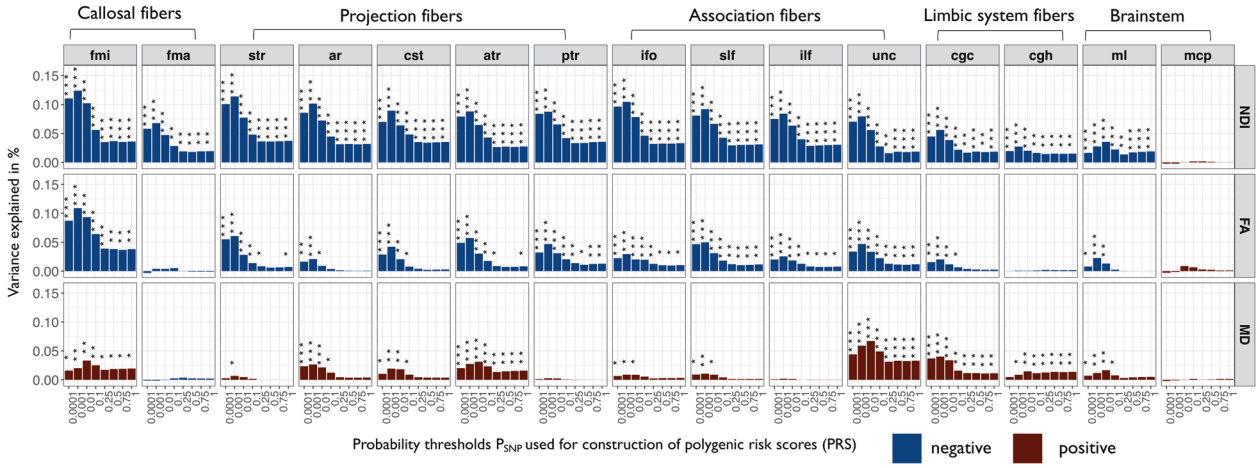

Fig. 5 Associations between polygenic risk scores for schizophrenia and white matter tracts. Barcharts of variance explained by schizophrenia PRS (R^2, *y*-axis) constructed at each of eight probability thresholds ($0.0001 \geq P_{SNP} \leq 1$, *x*-axis) for each of three white matter metrics (NDI neurite density index, FA fractional anisotropy, MD mean diffusivity) measured at 15 major white matter tracts: mcp middle cerebellar peduncle, ml medial lemniscus, cst corticospinal tract, ar acoustic radiation, atr anterior thalamic radiation, str superior thalamic radiation, pts posterior thalamic radiation, slf superior longitudinal fasciculus, ilf inferior longitudinal fasciculus, ifo inferior fronto-occipital fasciculus, unc uncinate fasciculus, cgc cingulate gyrus part of cingulum, cgh parahippocampal part of cingulum, fmi forceps minor, and fma forceps major. Blue bars indicate negative associations and red bars positive associations; asterisks indicate *P* values for association after FDR correction: $^{*}P \leq 0.05$, $^{**}P \leq 0.01$, $^{***}P \leq 0.001$. Polygenic risk scores for schizophrenia were significantly associated with NDI, FA, and MD of multiple white matter tracts.

extra-cellular, and cerebro-spinal fluid—each of which has different diffusion properties. The intra-cellular compartment refers to the space bound by neurites and allows for the measurement of their density (NDI) and their spatial orientation (ODI) [57, 58]. In vivo estimates of NDI have been biologically validated by ex vivo, histological estimates of neurite density in mice [59], and correlated with cortical myelination in humans [58].

Thus, a reasonable interpretation of our results is that polygenic risk for schizophrenia in the general population is associated with decreased axonal and/or dendritic density in grey and white matter. While we cannot ascribe causality using the current methods, this interpretation is consistent with several lines of previous research in individuals with schizophrenia. First, schizophrenia case-control studies have reported abnormally decreased NDI in the cortex, hippocampus, and white matter [26, 35]. Second, postmortem studies have reported multiple abnormalities of neurite structure in schizophrenia, including reduced dendritic arborization [60], reduced spine density [60], reduced axonal myelination [61], and reduced oligodendrocytes [62]. Third, recent GWAS studies have identified risk genes for schizophrenia that are expressed in neurons and implicated in dendritic arborization and microcircuit formation, synaptic plasticity, and glutamatergic neurotransmission [4, 49, 63–65]. It is intriguing to speculate which individual risk genes might be most relevant to the relationship between PRS and reduced NDI but we cannot certainly resolve this question from these results. Fourth, locally reduced density of myelinated axons and dendrites will likely reflect atypical connectivity between brain structures [61, 66], as anticipated by long-standing theories of schizophrenia as a dysconnectivity syndrome [67–70].

Integration of genetic associations across cortical phenotypes

While NDI was the one most strongly associated with PRS, almost all other metrics (except CT) also showed some significant regional associations with genetic risk. We consider that this apparent pleiotropy of genetic effects on brain structure largely reflects correlations between the MRI metrics [27]. For example, NDI was positively correlated with FA, and both NDI and FA were negatively correlated with MD (Fig. 3A). This is not surprising because increased NDI restricts isotropic diffusion of protons in the tissue water compartment so that FA is increased and MD is decreased [27]. These three metrics are thus complementary measures of the same or similar tissue composition characteristics, which explains the anatomical co-localization of genetic effects on NDI, FA, and MD (Fig. 4). These co-localized, multi-metric associations with PRS were concentrated in auditory and lateral temporal cortex, prefrontal and orbito-frontal cortex, anterior cingulate cortex, and insular cortical areas, many of which have previously been reported to show increased MD and/or decreased FA in case-control studies of schizophrenia [12, 23, 28–31].

Of the macrostructural phenotypes, LGI was positively correlated with MD and positively associated with genetic risk for schizophrenia. Local gyrification is assumed to capture early neurodevelopmental changes that are relatively stable after birth [25, 71]. Case-control data have recently shown increased LGI in schizophrenia, interpreted as a marker of structural dysconnectivity [25]. It is uncertain whether polygenic effects on macrostructural markers are mechanistically distinct from the effects on NDI and related microstructural markers. However, microstructural MRI metrics were clearly more strongly associated with genetic risk for schizophrenia than the macrostructural metrics that have previously been investigated as candidate endophenotypes.

Genetic risk and subcortical structures

Atypicality in subcortical structures is a frequently reported finding in schizophrenia cases [11], and in their non-psychotic first-degree relatives [72], compared to healthy controls. However, this is the first study to identify significant associations between polygenic risk for schizophrenia and subcortical structures in a population sample.

NDI was again the MRI metric most sensitive to genetic association, especially in the thalamus, where PRS was significantly associated with reduced NDI. The thalamus plays a key role in cognitive and emotional processes that are clinically impaired in schizophrenia [73, 74]. Thalamic volume reductions [73] and abnormal functional connectivity between thalamus and cortex [75] have been previously reported in schizophrenia. The basal ganglia (putamen, pallidum and caudate nucleus) and the hippocampus also demonstrated PRS-related changes in NDI and related microstructural metrics. There was also a robust

(negative) association between PRS and hippocampal volume, consistent with extensively replicated case-control differences in hippocampal volume [11].

Genetic risk and white matter tracts

Abnormalities of white matter microstructure, consistent with aberrant inter-hemispheric, fronto-temporal, and cortico-thalamic connectivity, have been frequently reported in schizophrenia [13, 33]. We identified significant associations between genetic risk for schizophrenia and microstructural metrics in most of the major axonal tracts we measured, indicating that PRS is associated with widespread disruption or disorganization of white matter. The strongest effect was a negative association between PRS and NDI of the forceps minor, the anterior part of the corpus callosum, inter-hemispherically connecting the frontal lobes. However, PRS was also significantly associated with NDI, FA, and MD in intra-hemispheric association fibers, cortico-subcortical projection fibers, limbic system, and brainstem fibers, indicating that genetic risk for schizophrenia is associated with anatomically widespread disruption of white matter tracts.

Investigation of causality

Association between PRS and brain MRI metrics, however, statistically significant or anatomically plausible, is uninformative about the underlying direction of causality [6]. In post-hoc analyses restricted to a subset of the NDI metrics most strongly associated with schizophrenia, we used bidirectional Mendelian randomization to test for causal effects of schizophrenia on NDI metrics (MR(i)), and for causal effects of NDI metrics on schizophrenia (MR(ii)). We found no evidence for a significant causal effect of schizophrenia on global grey matter, cortical, subcortical, or white matter tract NDI metrics. We also did not find significant causal effects of any NDI metrics on schizophrenia using genetic instruments selected at a stringent GWAS-significant threshold of $P = 5 \times 10^{-8}$. However, we did find a significant, potentially causal relationship between lower NDI in the thalamus and increased risk for schizophrenia when we used a less stringent significance threshold to increase the number of genetic instruments and thus boost the power of MR analysis. We consider that this amounts to suggestive evidence that thalamic NDI may causally predict schizophrenia, consistent with the prior observation that thalamic NDI was the regional MRI metric most strongly and robustly associated with PRS for schizophrenia. However, we also consider that the sample size available for GWAS of NDI metrics was underpowered to identify sufficient instrumental variables at the conventional threshold for genome-wide significance (or to estimate genome-wide associations with sufficient efficiency for significant genetic correlation analysis). More definitive investigations of the causal relationship between MRI metrics and schizophrenia, on the basis of better genetic instruments defined by larger MRI samples, will be important to pursue in future [47].

Strengths and limitations

It is a strength that we used the largest GWAS to date to construct schizophrenia PRS at multiple P_{SNP}-value thresholds for inclusion of risk variants. We also used the largest and most methodologically diverse MRI dataset to date in order to assess PRS associations with brain structure. However, the diagnostic variance in schizophrenia explained by PRS is still relatively small (7.7%) [4] and, in line with previous findings [18, 22], the proportion of variance in cortical and subcortical structures explained by the PRS is even smaller (<1%). It is expected that even larger sample sizes in future studies might implicate other brain structures or MRI metrics than those significantly associated with PRS in this study [4]. The reported results should be more robustly assessed by future translational MRI and histological studies of grey and white matter microstructure in human postmortem data or animal models of genetic risk for schizophrenia. Finally, the UK Biobank is an ageing cohort of largely European descent that is on average wealthier and healthier than the general population [76]. The generalisabilty of these results should be investigated in more demographically diverse and epidemiologically relevant samples.

Summary

PRS for schizophrenia were most robustly associated with significant changes in microstructural MRI metrics in the cortex, the subcortex, and white matter tracts, in a large population sample. These results provide substantial new evidence in support of the pathogenic model that genetic risk for schizophrenia is associated with reduced neurite density, and anatomical dysconnectivity, in cortico-subcortical networks.

DATA AVAILABILITY

Imaging and genetic data may be requested through the UK Biobank database (https://www.ukbiobank.ac.uk/). Summary level data for schizophrenia can be accessed from the Psychiatric Genomics Consortium (https://www.med.unc.edu/pgc/).

CODE AVAILABILITY

Any code used to generate derived data is shared on GitHub (https://github.com/ucam-department-of-psychiatry/UKB).

REFERENCES

1. Hilker R, Helenius D, Fagerlund B, Skytthe A, Christensen K, Werge TM, et al. Heritability of schizophrenia and schizophrenia spectrum based on the nationwide Danish twin register. Biol Psychiatry. 2018;83:492–8.
2. Sullivan PF, Kendler KS, Neale MC. Schizophrenia as a complex trait: evidence from a meta-analysis of twin studies. Arch Gen Psychiatry. 2003;60:1187–92.
3. Pardiñas AF, Holmans P, Pocklington AJ, Escott-Price V, Ripke S, Carrera N, et al. Common schizophrenia alleles are enriched in mutation-intolerant genes and in regions under strong background selection. Nat Genet. 2018;50:381–9.
4. Schizophrenia Working Group of the Psychiatric Genomics Consortium, Ripke, S., Walters, J.T.R & O'Donovan, M.C. Mapping genomic loci prioritises genes and implicates synaptic biology in schizophrenia. Preprint at medRxiv. 2020. https://doi.org/10.1101/2020.09.12.20192922.
5. Riglin L, Collishaw S, Richards A, Thapar AK, Maughan B, O'Donovan MC, et al. Schizophrenia risk alleles and neurodevelopmental outcomes in childhood: a population-based cohort study. Lancet Psychiatry. 2017;4:57–62.
6. Smeland OB, Frei O, Dale AM, Andreassen OA. The polygenic architecture of schizophrenia—rethinking pathogenesis and nosology. Nat. Rev. Neurol. 2020;16:366–79.
7. Gottesman II, Gould TD. The endophenotype concept in psychiatry: etymology and strategic intentions. Am J Psychiatry. 2003;160:636–45.
8. Fornito A, Bullmore ET. Connectomic intermediate phenotypes for psychiatric disorders. Front Psychiatry. 2012;3.
9. Bigos KL, Weinberger DR. Imaging genetics—days of future past. Neuroimage. 2010;53:804–9.
10. Bogdan R, Salmeron BJ, Carey CE, Agrawal A, Calhoun VD, Garavan H, et al. Imaging genetics and genomics in psychiatry: a critical review of progress and potential. Biol Psychiatry. 2017;82:165–75.
11. van Erp TGM, Hibar DP, Rasmussen JM, Glahn DC, Pearlson GD, Andreassen OA, et al. Subcortical brain volume abnormalities in 2028 individuals with schizophrenia and 2540 healthy controls via the ENIGMA consortium. Mol Psychiatry. 2016;21:547–53.
12. Van Erp TGM, Walton E, Hibar DP, Schmaal L, Jiang W, Glahn DC, et al. Cortical brain abnormalities in 4474 individuals with schizophrenia and 5098 control subjects via the Enhancing Neuro Imaging Genetics Through Meta Analysis (ENIGMA) Consortium. Biol Psychiatry. 2018;84:644–54.
13. Kelly S, Jahanshad N, Zalesky A, Kochunov P, Agartz I, Alloza C, et al. Widespread white matter microstructural differences in schizophrenia across 4322 individuals: results from the ENIGMA Schizophrenia DTI Working Group. Mol Psychiatry. 2018;23:1261–9.
14. Satizabal CL, Adams HHH, Hibar DP, White CC, Knol MJ, Stein JL, et al. Genetic architecture of subcortical brain structures in 38,851 individuals. Nat Genet. 2019;51:1624–36.
15. Grasby KL, Jahanshad N, Painter JN, Colodro-Conde Li, A, Bralten J, Hibar DP, et al. The genetic architecture of the human cerebral cortex. Science. 2020;367.

16. Kochunov P, Jahanshad N, Marcus D, Winkler A, Sprooten E, Nichols TE, et al. Heritability of fractional anisotropy in human white matter: a comparison of Human Connectome Project and ENIGMA-DTI data. Neuroimage. 2015;111:300–11.
17. van der Merwe C, Passchier R, Mufford M, Ramesar R, Dalvie S, Stein DJ. Polygenic risk for schizophrenia and associated brain structural changes: a systematic review. Compr Psychiatry. 2019;88:77–82.
18. Reus LM, Shen X, Gibson J, Wigmore E, Ligthart L, Adams MJ, et al. Association of polygenic risk for major psychiatric illness with subcortical volumes and white matter integrity in UK Biobank. Sci Rep. 2017;7:42140.
19. Franke B, Stein JL, Ripke S, Anttila V, Hibar DP, Van Hulzen KJE, et al. Genetic influences on schizophrenia and subcortical brain volumes: large-scale proof of concept. Nat Neurosci. 2016;19:420–31.
20. Grama S, Willcocks I, Hubert JJ, Pardiñas AF, Legge SE, Bracher-Smith M, et al. Polygenic risk for schizophrenia and subcortical brain anatomy in the UK Biobank cohort. Transl Psychiatry. 2020;10:1–10.
21. Van Scheltinga AFT, Bakker SC, Van Haren NEM, Derks EM, Buizer-Voskamp JE, Boos HBM, et al. Genetic schizophrenia risk variants jointly modulate total brain and white matter volume. Biol Psychiatry. 2013;73:525–31.
22. Neilson E, Shen X, Cox SR, Clarke T-K, Wigmore EM, Gibson J, et al. Impact of polygenic risk for schizophrenia on cortical structure in UK Biobank. Biol Psychiatry. 2019;86:536–44.
23. Ellison-Wright I, Bullmore E. Anatomy of bipolar disorder and schizophrenia: a meta-analysis. Schizophr Res. 2010;117:1–12.
24. Ronan L, Voets NL, Hough M, Mackay C, Roberts N, Suckling J, et al. Consistency and interpretation of changes in millimeter-scale cortical intrinsic curvature across three independent datasets in schizophrenia. Neuroimage. 2012;63:611–21.
25. Sasabayashi D, Takayanagi Y, Takahashi T, Nemoto K, Furuichi A, Kido M, et al. Increased brain gyrification in the schizophrenia spectrum. Psychiatry Clin Neurosci. 2020;74:70–76.
26. Nazeri A, Mulsant BH, Rajji TK, Levesque ML, Pipitone J, Stefanik L, et al. Gray matter neuritic microstructure deficits in schizophrenia and bipolar disorder. Biol Psychiatry. 2017;82:726–36.
27. Fukutomi H, Glasser MF, Murata K, Akasaka T, Fujimoto K, Yamamoto T, et al. Diffusion tensor model links to neurite orientation dispersion and density imaging at high b-value in cerebral cortical gray matter. Sci Rep. 2019;9:1–12.
28. McKenna FF, Miles L, Babb JS, Goff DC, Lazar M. Diffusion kurtosis imaging of gray matter in schizophrenia. Cortex. 2019;121:201–24.
29. Narr KL, Hageman N, Woods RP, Hamilton LS, Clark K, Phillips O, et al. Mean diffusivity: a biomarker for CSF-related disease and genetic liability effects in schizophrenia. Psychiatry Res. 2009;171:20–32.
30. Spoletini I, Cherubini A, Banfi G, Rubino IA, Peran P, Caltagirone C, et al. Hippocampi, thalami, and accumbens microstructural damage in schizophrenia: a volumetry, diffusivity, and neuropsychological study. Schizophr. Bull. 2011;37:118–30.
31. Kalus P, Slotboom J, Gallinat JU, rgen, Federspiel A, Gralla J, Remonda L, et al. New evidence for involvement of the entorhinal region in schizophrenia: a combined MRI volumetric and DTI study. Neuroimage. 2005;24:1122–9.
32. Woodward N, Parvatheni P. M82. Neurite orientation dispersion and density imaging (NODDI) of the prefrontal cortex in psychosis. Schizophr Bull. 2017;43:S240.
33. Ellison-Wright I, Bullmore E. Meta-analysis of diffusion tensor imaging studies in schizophrenia. Schizophr Res. 2009;108:3–10.
34. Kraguljac NV, Monroe WS, Anthony T, Jindal RD, Hill H, Lahti AC. Neurite Orientation Dispersion and Density Imaging (NODDI) and duration of untreated psychosis in antipsychotic medication-naïve first episode psychosis patients. Neuroimage. 2021;1:100005.
35. Rae CL, Davies G, Garfinkel SN, Gabel MC, Dowell NG, Cercignani M, et al. Deficits in neurite density underlie white matter structure abnormalities in first-episode psychosis. Biol Psychiatry. 2017;82:716–25.
36. Sudlow C, Gallacher J, Allen N, Beral V, Burton P, Danesh J, et al. UK biobank: an open access resource for identifying the causes of a wide range of complex diseases of middle and old age. PLoS Med. 2015;12.
37. Alfaro-Almagro F, Jenkinson M, Bangerter NK, Andersson JLR, Griffanti L, Douaud Ge LLE, et al. Image processing and quality control for the first 10,000 brain imaging datasets from UK Biobank. Neuroimage. 2018;166:400–24.
38. Fischl B, van der Kouwe A, Destrieux C, Halgren E, Ségonne F, Salat DH, et al. Automatically parcellating the human. Cereb Cortex Cereb Cortex. 2004;14:11–22.
39. Glasser MF, Coalson TS, Robinson EC, Hacker CD, Harwell J, Yacoub E, et al. A multi-modal parcellation of human cerebral cortex. Nature. 2016;536:171–8.
40. Daducci A, Canales-Rodr EJ, Zhang H, Dyrby TB, Alexander DC, Thiran J-P. Accelerated microstructure imaging via convex optimization (AMICO) from diffusion MRI data. NeuroImage. 2015;105:32–44.
41. De Groot M, Vernooij MW, Klein S, Ikram MA, Vos FM, Smith SM, et al. Improving alignment in tract-based spatial statistics: evaluation and optimization of image registration. Neuroimage. 2013;76:400–11.
42. Bycroft C, Freeman C, Petkova D, Band G, Elliott LT, Sharp K, et al. The UK Biobank resource with deep phenotyping and genomic data. Nature. 2018;562:203–9.
43. Yang J, Lee SH, Goddard ME, Visscher PM. GCTA: a tool for genome-wide complex trait analysis. Am J Hum Genet. 2011;88:76–82.
44. Martin AR, Daly MJ, Robinson EB, Hyman SE, Neale BM. Predicting polygenic risk of psychiatric disorders. Biol Psychiatry. 2019;86:97–109.
45. Warrier V, Baron-Cohen S. Childhood trauma, life-time self-harm, and suicidal behaviour and ideation are associated with polygenic scores for autism. Mol Psychiatry. 2021;26:1670–84.
46. Choi SW, O'Reilly PF. PRSice-2: Polygenic Risk Score software for biobank-scale data. Gigascience 2019;8:giz082.
47. Shen X, Howard DM, Adams MJ, Hill WD, Clarke T-K, Deary IJ, et al. A phenome-wide association and Mendelian Randomisation study of polygenic risk for depression in UK Biobank. Nat Commun. 2020;11:1–16.
48. Privé F, Vilhjálmsson BJ, Aschard H, Blum MGB. Making the most of clumping and thresholding for polygenic scores. Am J Hum Genet. 2019;105:1213–21.
49. Ripke S, Neale BM, Corvin A, Walters JTR, Farh K-H, Holmans PA, et al. Biological insights from 108 schizophrenia-associated genetic loci. Nature. 2014;511:421–7.
50. Smith SM, Nichols TE. Statistical challenges in "big data" human neuroimaging. Neuron. 2018;97:263–8.
51. Shen X, Reus LM, Cox SR, Adams MJ, Liewald DC, Bastin ME, et al. Subcortical volume and white matter integrity abnormalities in major depressive disorder: findings from UK Biobank imaging data. Sci Rep. 2017;7:1–10.
52. Hemani G, Zheng J, Elsworth B, Wade KH, Haberland V, Baird D, et al. The MR-Base platform supports systematic causal inference across the human phenome. elife. 2018;7:e34408.
53. Jiang L, Zheng Z, Qi T, Kemper KE, Wray NR, Visscher PM, et al. A resource-efficient tool for mixed model association analysis of large-scale data. Nat Genet. 2019;51:1749–55.
54. Gage SH, Jones HJ, Burgess S, Bowden J, Smith GD, Zammit S, et al. Assessing causality in associations between cannabis use and schizophrenia risk: a two-sample Mendelian randomization study. Psychological Med. 2017;47:971–80.
55. Bowden J, Davey, Smith G, Haycock PC, Burgess S. Consistent estimation in Mendelian randomization with some invalid instruments using a weighted median estimator. Genet Epidemiol. 2016;40:304–14.
56. Bulik-Sullivan B, Finucane HK, Anttila V, Gusev A, Day FR, Loh P-R, et al. An atlas of genetic correlations across human diseases and traits. Nat Genet. 2015;47:1236–41.
57. Zhang H, Schneider T, Wheeler-Kingshott CA, Alexander DC. NODDI: practical in vivo neurite orientation dispersion and density imaging of the human brain. Neuroimage. 2012;61:1000–16.
58. Fukutomi H, Glasser MF, Zhang H, Autio JA, Coalson TS, Okada T, et al. Neurite imaging reveals microstructural variations in human cerebral cortical gray matter. Neuroimage. 2018;182:488–99.
59. Gong N-J, Dibb R, Pletnikov M, Benner E, Liu C. Imaging microstructure with diffusion and susceptibility MR: neuronal density correlation in Disrupted-in-Schizophrenia-1 mutant mice. NMR Biomed. 2020;33:e4365.
60. Moyer CE, Shelton MA, Sweet RA. Dendritic spine alterations in schizophrenia. Neurosci Lett. 2015;601:46–53.
61. Flynn SW, Lang DJ, Mackay AL, Goghari V, Vavasour IM, Whittall KP, et al. Abnormalities of myelination in schizophrenia detected in vivo with MRI, and post-mortem with analysis of oligodendrocyte proteins. Mol Psychiatry. 2003;8:811–20.
62. Raabe FJ, Slapakova L, Rossner MJ, Cantuti-Castelvetri L, Simons M, Falkai PG, et al. Oligodendrocytes as a new therapeutic target in schizophrenia: from histopathological findings to neuron-oligodendrocyte interaction. Cells. 2019;8:1496.
63. Sekar A, Bialas AR, de Rivera H, Davis A, Hammond TR, Kamitaki N, et al. Schizophrenia risk from complex variation of complement component 4. Nature. 2016;530:177–83.
64. Harrison PJ, Weinberger DR. Schizophrenia genes, gene expression, and neuropathology: on the matter of their convergence. Mol Psychiatry. 2005;10:40–68.
65. Stephan KE, Friston KJ, Frith CD. Dysconnection in schizophrenia: from abnormal synaptic plasticity to failures of self-monitoring. Schizophrenia Bull. 2009;35:509–27.
66. Alexander-Bloch AF, Reiss PT, Rapoport J, McAdams H, Giedd JN, Bullmore ET, et al. Abnormal cortical growth in schizophrenia targets normative modules of synchronized development. Biol Psychiatry. 2014;76:438–46.
67. Morgan SE, Seidlitz J, Whitaker KJ, Romero-Garcia R, Clifton NE, Scarpazza C, et al. Cortical patterning of abnormal morphometric similarity in psychosis is associated with brain expression of schizophrenia-related genes. Proc Natl Acad Sci USA. 2019;116:9604–9.
68. Nelson BG, Bassett DS, Camchong J, Bullmore ET, Lim KO. Comparison of large-scale human brain functional and anatomical networks in schizophrenia. NeuroImage. 2017;15:439–48.
69. Schmitt A, Hasan A, Gruber O, Falkai P. Schizophrenia as a disorder of disconnectivity. Eur Arch Psychiatry Clin Neurosci. 2011;261:150.
70. Friston KJ, Frith CD. Schizophrenia: a disconnection syndrome. Clin Neurosci. 1995;3:89–97.
71. Zilles K, Palomero-Gallagher N, Amunts K. Development of cortical folding during evolution and ontogeny. Trends Neurosci. 2013;36:275–84.

72. McIntosh AM, Job DE, Moorhead TWJ, Harrison LK, Forrester K, Lawrie SM, et al. Voxel-based morphometry of patients with schizophrenia or bipolar disorder and their unaffected relatives. Biol Psychiatry. 2004;56:544–52.
73. Pergola G, Selvaggi P, Trizio S, Bertolino A, Blasi G. The role of the thalamus in schizophrenia from a neuroimaging perspective. Neurosci Biobehav Rev. 2015;54:57–75.
74. Wagner G, Koch K, Schachtzabel C, Schultz CC, Gaser C, Reichenbach JU, et al. Structural basis of the fronto-thalamic dysconnectivity in schizophrenia: a combined DCM-VBM study. NeuroImage. 2013;3:95–105.
75. Chen P, Ye E, Jin X, Zhu Y, Wang L. Association between thalamocortical functional connectivity abnormalities and cognitive deficits in schizophrenia. Sci Rep. 2019;9:1–10.
76. Fry A, Littlejohns TJ, Sudlow C, Doherty N, Adamska L, Sprosen T, et al. Comparison of sociodemographic and health-related characteristics of UK Biobank participants with those of the general population. Am J Epidemiol. 2017;186:1026–34.

ACKNOWLEDGEMENTS

E-MS is supported by a Ph.D. studentship awarded by the Friends of Peterhouse. This research was co-funded by the National Institute of Health Research (NIHR) Cambridge Biomedical Research Centre and a Marmaduke Sheild grant to RAIB and VW. ETB is an NIHR Senior Investigator. RRG was funded by a Guarantors of Brain Fellowship. RAIB is supported by a British Academy Post-Doctoral fellowship and the Autism Research Trust. We wish to thank Dr. Petra Vértes and Dr. Lisa Ronan for their advice on research design and Dr. Simon R White for his statistical advice and support. The views expressed are those of the author(s) and not necessarily those of the NHS, the NIHR, or the Department of Health and Social Care. This research was possible due to an application to the UK Biobank (project 20904).

AUTHOR CONTRIBUTIONS

E-MS, RAIB, VW, GKM, and ETB designed research. JS advised on research design. E-MS, RAIB, VW, and RRG analyzed data. E-MS and RAIB made figures. E-MS, RAIB, and VW performed research. E-MS and ETB wrote the paper.

COMPETING INTERESTS

ETB serves on the Scientific Advisory Board of Sosei Heptares and as a consultant for GlaxoSmithKline. All other authors declare no conflicts of interest.

ADDITIONAL INFORMATION

Supplementary information The online version contains supplementary material available at https://doi.org/10.1038/s41380-021-01260-5.

Correspondence and requests for materials should be addressed to E.-M.S.

Reprints and permission information is available at http://www.nature.com/reprints

Publisher's note Springer Nature remains neutral with regard to jurisdictional claims in published maps and institutional affiliations.

Open Access This article is licensed under a Creative Commons Attribution 4.0 International License, which permits use, sharing, adaptation, distribution and reproduction in any medium or format, as long as you give appropriate credit to the original author(s) and the source, provide a link to the Creative Commons license, and indicate if changes were made. The images or other third party material in this article are included in the article's Creative Commons license, unless indicated otherwise in a credit line to the material. If material is not included in the article's Creative Commons license and your intended use is not permitted by statutory regulation or exceeds the permitted use, you will need to obtain permission directly from the copyright holder. To view a copy of this license, visit http://creativecommons.org/licenses/by/4.0/.

© The Author(s) 2021